Article

Revealing the Structure of Single Cobalt Sites in Carbon Nitride for Photocatalytic CO_2 Reduction

Peipei Huang, Jiahao Huang, Junying Li, Thang Duc Pham, Lei Zhang, Jie He, Gary W. Brudvig, N. Aaron Deskins,* Anatoly I. Frenkel,* and Gonghu Li*

Read Online
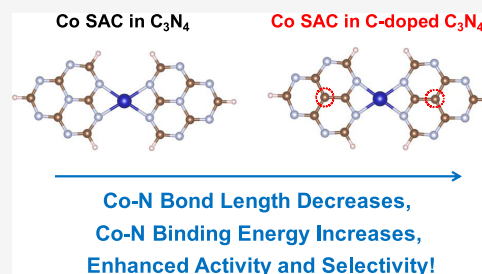
ACCESS | 📊 Metrics & More | 📄 Article Recommendations | 🔵SI Supporting Information

ABSTRACT: Single Co^{2+} sites in graphitic carbon nitride (C_3N_4) have demonstrated excellent activity and selectivity in photocatalytic CO_2 reduction. In this work, we combine computational and spectroscopic tools, including X-ray absorption spectroscopy, to probe the structure of such single Co^{2+} sites. Our results indicate that the Co^{2+} sites exist in the $Co-N_{2+2}$ coordination at the edges of C_3N_4 flakes. This mode of coordination is further supported by experimental results obtained using single Co^{2+} sites in C_3N_4 materials treated with NH_3, which contain more edge sites than untreated C_3N_4. In our experimental observations, doping C_3N_4 with carbon is found to be important for the photocatalytic properties of the single Co^{2+} sites. A simplified model is proposed to explain the origin of the observed enhancement effect of C doping. In this model, the presence of C dopant near the metal centers results in shorter Co−N bond length and stronger Co−N binding energy. In addition to enhanced light absorption and charge separation in C-doped C_3N_4, the stronger Co−N binding upon C doping likely contributes to the improved catalytic properties of the single Co^{2+} sites.

Co SAC in C_3N_4 Co SAC in C-doped C_3N_4

Co-N Bond Length Decreases, Co-N Binding Energy Increases, Enhanced Activity and Selectivity!

1. INTRODUCTION

Single-atom catalysts (SACs) exhibit distinct properties for a wide range of chemical reactions and allow the use of characterization techniques available in both heterogeneous and homogeneous catalysis.[1−6] This type of catalyst has been extensively explored in a variety of applications, including electrocatalysis[7,8] and photocatalysis.[9] SACs confined in single layers of two-dimensional (2D) materials could offer unique properties. A variety of 2D materials, including N-doped graphene and graphitic carbon nitride (C_3N_4), have been employed as support for SACs.[5,10−12] For SACs in such materials, metal (M)-N coordination was found to be key to their catalytic activities. For example, the presence of Ni−N_4 sites in a carbon-based electrode was shown to account for the excellent activity and product selectivity toward CO_2 reduction.[13,14]

The structure of C_3N_4, which has a band gap of 2.7 eV and can harvest visible light (up to 460 nm),[15] enables it to serve as a photoactive support for SACs.[10,16−20] In CO_2 reduction, C_3N_4 materials have been studied as photocatalysts by themselves,[21] or coupled with metal−ligand complexes[22−26] to achieve enhanced catalysis. A few studies, including our recent work,[27] have examined SACs in C_3N_4 for use in photocatalytic CO_2 reduction.[28−36] Despite the strong interest in this area, the exact structures of SACs in C_3N_4 remain under debate. Existing models in the literature include in-plane M-N_3 and inter-layer M-N_4 coordination,[37] C-M-N_2 coordination,[28]

M-N_4 coordination in the presence of N vacancies,[38] and other possible structures.[39,40]

Recently, we prepared Co SACs in C_3N_4 that demonstrated excellent activity and product selectivity in photocatalytic CO_2 reduction.[27] However, the exact structure of such Co SACs remains elusive.[41−45] In this current work, we combine experimental and computational studies to investigate the structure of Co SACs in C_3N_4. Specifically, the Co SACs were characterized using different techniques, including X-ray absorption near edge structure (XANES) and extended X-ray absorption fine structure (EXAFS) spectroscopies. Binding of Co atoms to C_3N_4 was simulated using density functional theory (DFT). The obtained results were utilized to confirm the structure of the Co SACs. In addition, doping C_3N_4 with carbon was found to be important for the observed photocatalytic properties of the Co SACs in C_3N_4. Herein, we also explore the origin of such enhancement effects of C doping.
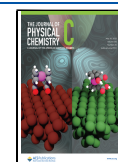
2. EXPERIMENTAL SECTION

2.1. Materials. Acetonitrile (99.999%), 1,4,8,11-tetraaza-cyclotetradecane (Cyclam, 98%), and cobalt(II) chloride were obtained from Sigma-Aldrich. Urea (99.5+%) and dextrose (anhydrous) were purchased from Fisher Chemical. Methanol and chloroform (99.8%) were purchased from Pharmco-Aaper. Triethylamine (TEA, ≥99%) was obtained from Acros. Triethanolamine (TEOA, ≥99%) was obtained from Alfa Aesar. All reagents were used without further purification.

2.2. Synthesis of C_3N_4, C-C_3N_4, and NH_3-Treated Samples. Graphitic carbon nitride (C_3N_4) was prepared by pyrolysis of urea. In a typical synthesis, 20 g of urea (99.5+% purity) was put into a covered crucible and calcined in a muffle furnace at 600 °C for 4 h (ramp rate 5 °C/min). In one of our previous studies on Co SACs,[27] C-doped C_3N_4 was obtained using a urea sample of 98% purity. However, the quality of C-doped C_3N_4 may vary due to differences in the composition of commercial urea samples at this purity level. Recently, we reported an improved method to synthesize Co SACs using urea of the highest purity (99.5+%) and dextrose as the source of C dopant.[46] In this current study, Co SACs in C-doped C_3N_4 were synthesized following the improved method. In particular, 20 mg of dextrose was evenly ground with the urea (the total mass was kept at 20 g) as the precursor. The obtained sample was denoted as C-C_3N_4. Both C_3N_4 and C-C_3N_4 were also treated with NH_3, in which a 1 g sample was put into a partially covered crucible and calcined in a tube furnace at 500 °C for 4 h (ramp rate 5 °C/min) with the flow of NH_3 (94 mL/min). The resulting materials were denoted as NH_3-C_3N_4 and NH_3-C-C_3N_4, respectively.

2.3. Synthesis of Single Co^{2+} Sites on Various C_3N_4 Samples. Single Co^{2+} sites were prepared through a microwave method. In a typical synthesis, 100 mg of C_3N_4 was mixed with 1.25 mg of $CoCl_2$ in 7.5 mL of acetonitrile and then stirred for 2 h. The mixture in a capped reaction vessel was placed in a CEM Discover single-mode microwave reactor and was heated to 80 °C for 120 min. After the microwave reaction, the resulting precipitate was recovered by centrifugation and washed several times with acetonitrile. After drying at room temperature, a hybrid photocatalyst, denoted as $Co^{2+}@C_3N_4$, was obtained. Following the same procedure, $Co^{2+}@C$-C_3N_4, $Co^{2+}@NH_3$-C_3N_4, and High-$Co^{2+}@NH_3$-C_3N_4 were also synthesized. A sample with low cobalt loading, Low-$Co^{2+}@NH_3$-C-C_3N_4, was synthesized in the presence of 0.04 mg of $CoCl_2$ and 100 mg of NH_3-C-C_3N_4.

2.4. Synthesis of Co Cyclam/C_3N_4 and Co Cyclam/C-C_3N_4. A molecular CO_2-reduction catalyst, [Co(cyclam)Cl_2]Cl (denoted "Co Cyclam"), was deposited on C_3N_4 and C-C_3N_4 following an established method.[47] In a typical synthesis, 100 mg of C_3N_4 was mixed with 1.5 mg of [Co(cyclam)Cl_2]Cl in 7.5 mL of acetonitrile and 65 μL of TEA and then stirred for 2 h. The mixture in a capped reaction vessel was placed in a CEM Discover single-mode microwave reactor and was heated to 80 °C for 120 min. After the microwave reaction, the resulting precipitate was recovered by centrifugation and washed twice with chloroform, methanol, and acetonitrile, respectively. After drying at room temperature, a hybrid photocatalyst, denoted as Co Cyclam/C_3N_4, was obtained. Following the same procedure, another hybrid photocatalyst, denoted as Co Cyclam/C-C_3N_4, was also obtained.

2.5. Materials Characterization. Elemental analysis of cobalt was conducted by acid digestion, followed by quantification using a Varian Vista AX induced coupled plasma-atomic emission spectrometer. X-ray diffraction (XRD) patterns of powder samples were collected on a Rigaku XDS 2000 diffractometer using nickel-filtered Cu Kα radiation (λ = 1.5418 Å). Scanning electron microscopy (SEM) images were collected on an Amray 3300FE field emission SEM with PGT Imix-PC microanalysis system. UV−visible spectra were obtained on a Cary 50 Bio spectrophotometer. A Barrelino diffuse reflectance probe was used to collect UV−visible spectra of powder samples using $BaSO_4$ as a standard. Transmission FTIR spectra were collected on a Thermo Nicolet iS10 FTIR spectrometer. The surface areas were measured by the Brunauer−Emmett−Teller (BET) method using N_2 adsorption/desorption on an Autosorb-1 analyzer (Quantachrome Instruments). Photoluminescence (PL) spectra were collected on a Cary Eclipse fluorescence spectrophotometer. Electron paramagnetic resonance (EPR) spectra were collected at liquid helium temperature on an X-band (9.5 GHz) Bruker EleXsys E-500 cw-EPR/ENDOR spectrometer.

2.6. X-ray Absorption Spectroscopy. X-ray absorption spectra at the Co K-edge were taken at the beamline 7-BM (QAS) of National Synchrotron Light Source II (NSLS-II) at Brookhaven National Laboratory. A Si(111) double crystal was used as a monochromator. A passivated implanted planar silicon (PIPS) detector was used for the detection of fluorescence from the samples. The beam size was 1.4 mm (vertical) × 6 mm (horizontal). The samples were made into 13 mm diameter pellets. All measurements were performed in the ambient atmosphere at room temperature, and the samples were held in 45° geometry. A Co foil was placed between the two detectors downstream from the sample and measured simultaneously with the sample as a reference for energy alignment. At least 25 scans were measured for each sample. The existing data for Co oxides were aligned with the samples' spectra using their respective reference foil spectra.

In our recent work,[46] EXAFS analysis was performed for each sample independently. In this work, due to the low cobalt loading of Low-$Co^{2+}@NH_3$-C-C_3N_4, the multiple data set fitting mode was used in the EXAFS analysis for all of the samples to reduce uncertainties in the Co−N distances and coordination numbers. The coordination number of Low-$Co^{2+}@NH_3$-C-C_3N_4 was constrained to vary together as the coordination number of $Co^{2+}@C$-C_3N_4. In addition to that, ΔE_0 is constrained to be the same for all samples. The best fit value of ΔE_0 was obtained to be -0.7 ± 0.6 eV.

2.7. Photocatalytic Testing. In photocatalytic CO_2 reduction, 1 mg of the catalyst was dispersed in a 4.0 mL mixture solution of acetonitrile containing TEOA (acetonitrile: TEOA = 4:1 v/v) as an electron donor in a quartz test tube. Prior to photocatalytic testing, the reaction solution was bubbled with CO_2 (99.999%, Airgas) in the dark for 20 min. The reaction solution was then irradiated with a halogen lamp equipped with a water filter. Light intensity on the reaction solution was fixed at 200 mW/cm². The head space above the reaction solution was sampled with a gas-tight syringe at different time intervals for product analysis using an Agilent 7820 GC equipped with a TCD detector and a 60:80 Carboxen-1000 packed column (Supelco).

2.8. Computational Methodology. Binding of Co atoms to C_3N_4 was simulated using the DFT code, the Vienna Ab initio Simulation Package (VASP).[48−51] We used projector augmented wave (PAW) potentials[52,53] for core electrons, and plane waves with a cutoff energy of 450 eV for valence

electrons. The Perdew−Burke−Ernzerhof (PBE) exchange-correlation functional[54] was employed. Gaussian smearing with a smearing width of 0.1 eV was used. The Grimme D3 correction with Becke-Johnson damping[55,56] was applied to include dispersion forces. All calculations were spin-polarized. Previous theoretical work[57,58] indicated that the tri-*s*-triazine structure is the most stable of possible C_3N_4 structures. This structure consists of 2D sheets with C and N atoms in a hexagonal array with an open cavity present in the sheets. We used this structure in the current work. A single sheet of C_3N_4 was modeled using a (1×1) cell having lattice lengths of 7.13 Å, as shown in Figure S1 in the Supporting Information. A $4 \times 4 \times 1$ *k*-point mesh was used for these sheet calculations. We placed Co atoms at various locations (i.e., on top of C/N atoms, bridging C/N atoms, within the cavity) and calculated binding energies of Co as the $E_{Co-C_3N_4} - E_{Co} - E_{C_3N_4}$. Here, $E_{Co-C_3N_4}$ is the energy of the Co-C_3N_4 complex, E_{Co} is the energy of a single Co atom, and $E_{C_3N_4}$ is the energy of the bare C_3N_4 sheet. We calculated the energies of Co with several spin states to find the most stable electron configuration of a single Co atom and modeled C-C_3N_4 sheets by replacing select N atoms in the sheets with C atoms. Finally, we also modeled the potential edges of C_3N_4. Such edges may be present in the sheets and may be reactive sites. These edges were modeled as clusters extracted from C_3N_4, similar to previous work.[59] We modeled Co interacting with one edge (one cluster) or two edges (two clusters). These clusters were modeled in a large box with a single *k*-point.

3. RESULTS AND DISCUSSION

In our study, pristine C_3N_4 was prepared from pyrolysis of urea. A Co SAC (denoted $Co^{2+}@C_3N_4$) was synthesized by depositing Co^{2+} cations in pristine C_3N_4 via a microwave method.[27] In photocatalytic CO_2 reduction, CO and H_2 were found to be the only gaseous products in the presence of triethanolamine as an electron donor. Under the experimental conditions employed in this study, $Co^{2+}@C_3N_4$ showed negligible activity toward CO_2 reduction while producing more H_2 than CO (Figures 1 and S2 and Table S1 in Supporting Information). In comparison, significantly higher

activity toward CO production was obtained using a Co SAC deposited in C-doped C_3N_4 (denoted $Co^{2+}@C-C_3N_4$, Figure 1), which was synthesized by pyrolysis of urea and a small amount of dextrose (0.1 wt %).[46] Furthermore, significantly higher selectivity toward CO formation was obtained using $Co^{2+}@C-C_3N_4$ (72%, Table 1) than using $Co^{2+}@C_3N_4$ (28%).

We have examined the Co SACs in C_3N_4 using X-ray absorption spectroscopy. The Co *K*-edge XANES and EXAFS spectra of $Co^{2+}@C_3N_4$ are very similar to those of $Co^{2+}@C-C_3N_4$ (Figure 2). As discussed in our previous work,[27] comparison of the XANES spectra with those of reference samples indicated the oxidation state of cobalt in the Co SACs is 2+. Further characterization using electron paramagnetic resonance spectroscopy indicated that both Co SACs contain high spin Co^{2+} (Figure S3). Our calculations also confirmed the high spin state of Co^{2+} (a magnetic moment of 2.037 μ_B on the Co atom). In the EXAFS spectra, the absence of high order contribution beyond the first peak is consistent with the dominance of single Co^{2+} sites in both $Co^{2+}@C_3N_4$ and $Co^{2+}@C-C_3N_4$. Fitting their EXAFS spectra (Figure S4) resulted in a coordination number of ~4 for both Co SACs, with four equivalent Co−N bonds having bond lengths of ~2.08 Å for $Co^{2+}@C_3N_4$ and ~2.07 Å for $Co^{2+}@C-C_3N_4$ (Table 1).

Computational modeling was conducted to explore the possible structures of $Co^{2+}@C_3N_4$. Binding of Co atoms to the N atoms in the C_3N_4 framework was investigated using DFT calculations. The modeling work failed to reach a Co SAC structure with four equivalent Co−N bonds inside the "pocket" of pristine C_3N_4 (Figure 3a,b; see also Table S2). Instead, a Co−N_{2+2} coordination at C_3N_4 edge sites appeared to be the most probable structure (Figure 3c) with a calculated binding energy of −358 kJ/mol (Table S3). In this structure, the calculated Co−N bond length is in the range of 2.07−2.10 Å (Table S3), in excellent agreement with the values obtained by fitting EXAFS spectra of the Co SAC (Table 1). This structure is supported by similar studies in the literature, such as the Fe-N_{2+2} sites of highly active Fe SACs confined in N-doped carbon materials.[60−62] In our study, this Co−N_{2+2} coordination at C_3N_4 edge sites is also the most probable structure for $Co^{2+}@C-C_3N_4$ (Table S3).

As shown in our previous work,[27] Co SACs only exist at very low loadings in C_3N_4; CoOx clusters and nanoparticles were produced at higher cobalt loadings. This can be explained by the fact that only a small amount of edge N sites are available in the C_3N_4 material, as compared to abundant framework N atoms in the "pockets," for coordination with Co^{2+}. To further validate the Co−N_{2+2} model for the Co SACs, pristine C_3N_4 and C-C_3N_4 were treated with gaseous NH_3 at elevated temperatures to create more edge sites. The resulting materials are denoted as NH_3-C_3N_4 and NH_3-C-C_3N_4, respectively. Figure 4 shows typical characterization results for C-C_3N_4 and NH_3-C-C_3N_4. Notably, smaller flakes are seen in NH_3-C-C_3N_4 than C-C_3N_4 (Figures 4d and S5). The photoluminescence spectra shown in Figure 4e suggest the presence of more edge defect sites in NH_3-C-C_3N_4 than in C-C_3N_4.

The NH_3 treatment significantly increased the surface areas of the C_3N_4 materials (Table S1) and also their capacity to coordinate Co^{2+} (Table 1) in the presence of the same amount of Co^{2+} precursor used in catalyst synthesis (1.25 mg $CoCl_2$). Despite the higher cobalt loadings, Co SACs in the NH_3-treated samples demonstrated higher activity than the samples without the treatment (Table 1 and Figure S6). These results
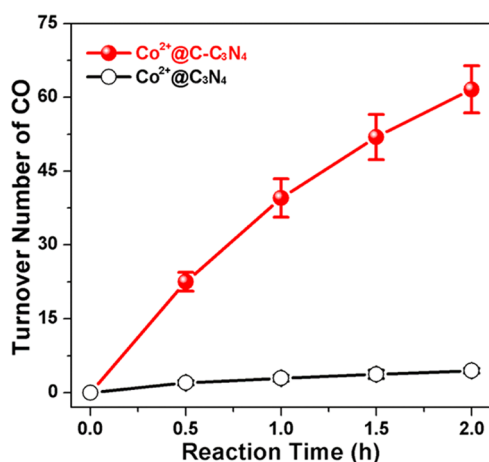

Figure 1. Production of CO using $Co^{2+}@C_3N_4$ (open cycle) and $Co^{2+}@C-C_3N_4$ (solid cycle) in photocatalytic CO_2 reduction under light irradiation ($\lambda > 350$ nm) in the presence of triethanolamine as an electron donor.

Table 1. Cobalt Loadings, Turnover Numbers (TON_{CO}), Selectivity Toward CO Formation, and EXAFS Spectra Fitting Results: Co−N Distances (d_{Co-N}) and Coordination Numbers (CN_{Co-N})

samples	Co loading ($\mu mol/g$)[a]	CO ($\mu mol/g$)	TON_{CO}[b]	selectivity for CO (%)[c]	d_{Co-N} (Å)[d]	CN_{Co-N}[d]
$Co^{2+}@C_3N_4$	14.6	65	4.4	28	2.08 ± 0.01	4.2 ± 0.9
$Co^{2+}@C-C_3N_4$	14.1	870	61.6	72	2.07 ± 0.01	4.2 ± 1.0
$Co^{2+}@NH_3-C_3N_4$	29.8	235	7.9	38	2.08 ± 0.01	4.6 ± 0.8
High-$Co^{2+}@NH_3-C-C_3N_4$	43.3	4026	93.0	80	2.07 ± 0.01	4.3 ± 0.5
Low-$Co^{2+}@NH_3-C-C_3N_4$	2.3	1895	818.9	74	2.03 ± 0.04	4.2

[a]Determined by elemental analysis. [b]TONs for CO after CO_2 reduction for 2 h. [c]Selectivity for CO formation calculated as the ratio between the amount of CO produced and the total amount of gaseous products (CO and H_2). [d]Results obtained from EXAFS spectra fitting.
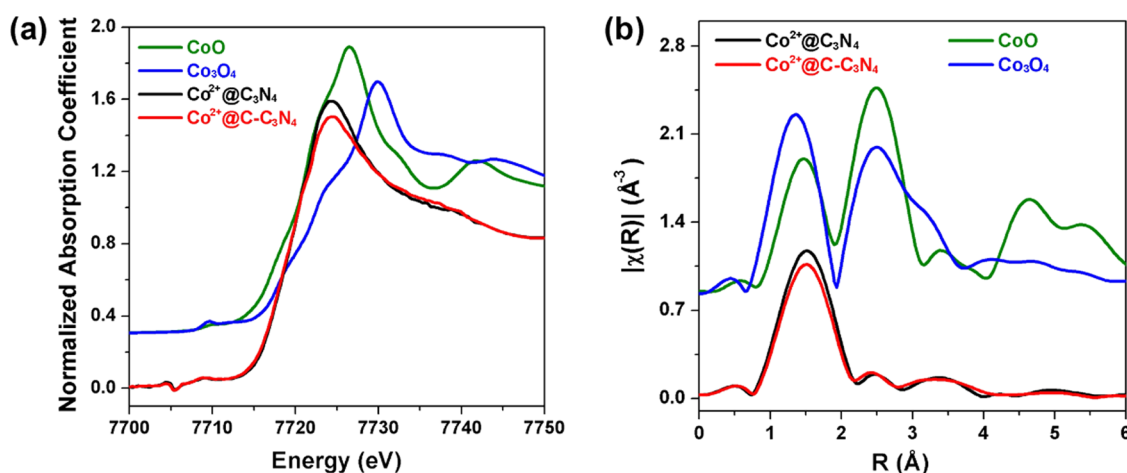
Figure 2. (a) Normalized Co K-edge XANES spectra and (b) Fourier transform magnitude of k^2-weighted Co K-edge EXAFS spectra of $Co^{2+}@C_3N_4$, $Co^{2+}@C-C_3N_4$, and reference samples (CoO and Co_3O_4). The k-range used in Fourier transform was from 2 to 7 Å^{-1}.
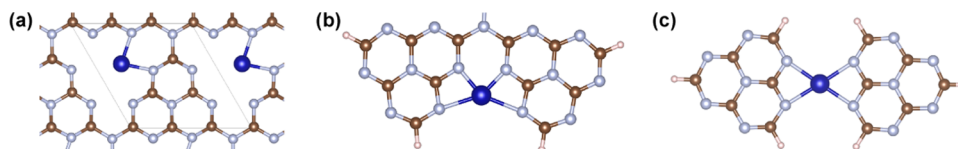
**Figure 3.** Structures of single Co^{2+} sites coordinated with N atoms in C_3N_4: (a) Co−N_2, (b) Co−N_4, and (c) Co−N_{2+2} at edge sites. Color scheme: Co (blue), N (silver), C (gold), and H (light brown).

obtained using the NH_3-treated samples strongly support the presence of single Co^{2+} sites at C_3N_4 edge sites in our Co SACs.

We further explored the origin of the observed differences in activity and selectivity of $Co^{2+}@C_3N_4$ and $Co^{2+}@C-C_3N_4$ (Table 1) by characterizing the synthesized materials with a variety of techniques. Pristine C_3N_4 and C-C_3N_4 show the same morphology, as can be seen from their microscopy images (see Figure S5). Pristine C_3N_4 and C-C_3N_4 containing Co SACs materials have similar surface areas and cobalt loadings (Tables 1 and S1). The synthesized C-C_3N_4 has a darker color and greater absorption than pristine C_3N_4 in the visible-light region (400−800 nm, Figure S7a). Furthermore, doping C_3N_4 with carbon significantly inhibited photoinduced charge recombination, as indicated by the comparison shown in the photoluminescence spectra of C-C_3N_4 and C_3N_4 (Figure S7b). It has been demonstrated that appropriate carbon doping can enhance the photocatalytic properties of C_3N_4 materials by improving its photoresponse in the visible region (400−800 nm)[46,63,64] and inhibiting charge recombination.[46,65−70] These differences should account for, at least partly, the observed higher activity of $Co^{2+}@C-C_3N_4$ than $Co^{2+}@C_3N_4$ in our study.

It appears that other reasons could also contribute to the enhanced activity of $Co^{2+}@C-C_3N_4$ in photocatalytic CO_2 reduction. This is based on our observations using hybrid photocatalysts consisting of Co Cyclam, where cyclam is 1,4,8,11-tetraazacyclotetradecane, deposited on the C_3N_4 materials following our established procedures (Figure S8).[25,47] Co Cyclam is a molecular CO_2-reduction catalyst that has a well-defined Co−N_4 coordination structure.[71,72] When the hybrid photocatalysts containing Co Cyclam were tested in CO_2 reduction, only a 2-fold enhancement in activity was obtained on C-C_3N_4 in comparison with C_3N_4 (Figure S9). This difference is likely due to the better light absorption and decreased charge recombination in C-C_3N_4. However, $Co^{2+}@C-C_3N_4$ demonstrated ~14 times higher activity than $Co^{2+}@C_3N_4$ in CO_2 reduction under the same experimental conditions (Table 1).

The above discussion of experimental results suggests that C doping likely affected the coordination environment of Co^{2+} sites in C-doped C_3N_4. We further carried out computational studies using a simplified structural model of C doping. In this model, two or more N atoms near the edge sites are replaced with C atoms upon C doping (Figure S1b,c). It should be pointed out that the exact location and structure of doped C
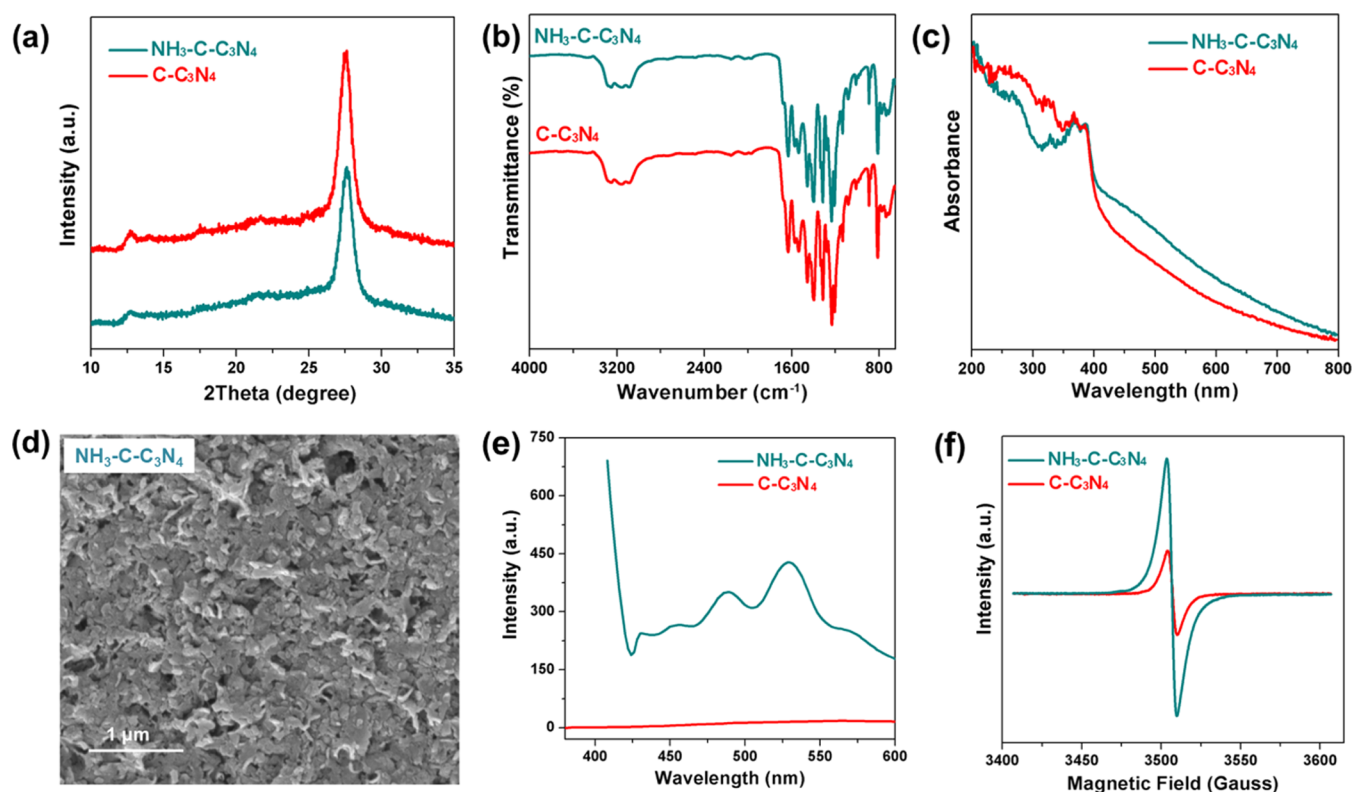
Figure 4. Characterization of NH_3-C-C_3N_4 and C-C_3N_4: (a) X-ray powder diffraction patterns, (b) infrared spectra, (c) UV−vis spectra, (d) a scanning electron micrograph, (e) photoluminescence spectra, and (f) electron paramagnetic resonance spectra.
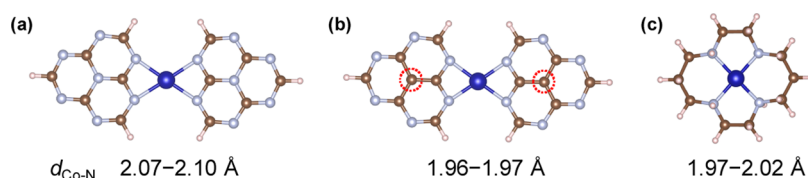

Figure 5. Calculated structures and Co−N bond lengths for (a) Co^{2+}@C_3N_4, (b) Co^{2+}@C-C_3N_4, and (c) Co Cyclam. In panel (c), Cl^- ligands are omitted for clarity.

atoms in our Co^{2+}@C-C_3N_4 sample are unclear, and this simplified structural model is employed in this study to understand the effect of C doping at the molecular level. Our computational calculations indicate that such substitution significantly strengthens Co−N coordination (Table S2). For the Co−N_{2+2} structure, C doping by replacing two N atoms near the edge sites led to stronger Co−N binding and a shorter bond length in Co^{2+}@C-C_3N_4 than in Co^{2+}@C_3N_4 (Figure 5 and Table S3). The stronger Co−N binding in Co^{2+}@C-C_3N_4 could alter the photocatalytic properties of the single Co^{2+} sites by enhancing electron transfer from the photoactivated C-C_3N_4 to the Co^{2+} center. Further DFT calculations are underway to investigate other possible structures of C doping and the mechanism of photocatalytic CO_2 reduction on Co^{2+}@C-C_3N_4.

The Co−N bond length in Co^{2+}@C-C_3N_4 was calculated to be 1.96−1.97 Å, much shorter than that obtained by fitting EXAFS spectra of Co^{2+}@C-C_3N_4 and High-Co^{2+}@NH_3-C-C_3N_4 (both ∼2.07 Å, Table 1). This discrepancy is likely due to the fact that most of the single Co^{2+} sites in these samples are located far from doped C atoms. This argument is supported by the fact that a much shorter Co−N bond (2.03 Å, Table 1) was obtained by analyzing the EXAFS spectrum of

a sample "Low-Co^{2+}@NH_3-C-C_3N_4," which was intentionally synthesized to have a low cobalt loading (Table 1). As can be seen from the EXAFS spectra of Co SACs in NH_3-C_3N_4 and NH_3-C-C_3N_4, the peak position for Co^{2+}@NH_3-C-C_3N_4 shifted to shorter distances compared to Co^{2+}@NH_3-C_3N_4. Fitting the EXAFS spectra (Figure S10) obtained evidence of 4-coordinated Co with shorter Co−N bond lengths in NH_3-C-C_3N_4 than in NH_3-C-C_3N_4, and such comparison is much more pronounced for the sample "Low-Co^{2+}@NH_3-C-C_3N_4," in agreement with visual observation of the spectra shown in Figure 6.

We note that the sample Low-Co^{2+}@NH_3-C-C_3N_4 exhibited an activity ∼9 higher than High-Co^{2+}@NH_3-C-C_3N_4 in photocatalytic CO_2 reduction under the same experimental conditions (Table 1). Meanwhile, the Co−N bond lengths obtained by fitting EXAFS spectra were 2.07 and 2.03 Å for High-Co^{2+}@NH_3-C-C_3N_4 and Low-Co^{2+}@NH_3-C-C_3N_4, respectively (Table 1). Based on the above discussion, there are more Co^{2+} sites in Low-Co^{2+}@NH_3-C-C_3N_4 than in High-Co^{2+}@NH_3-C-C_3N_4 that are coordinated with N atoms near the doped C atoms. This is due to the fact that at low loadings, the Co^{2+} ions would preferentially bond to N atoms near the doped C atoms (Co−N binding energy −741 kJ/mol, Table
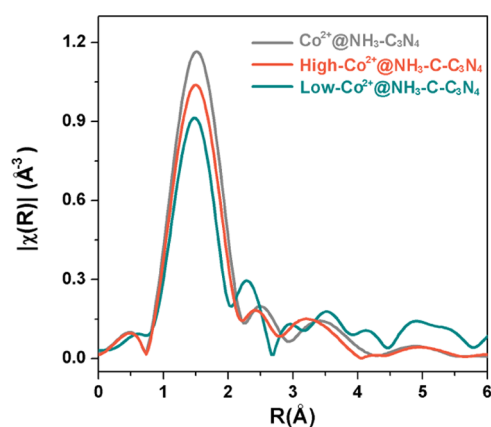
Figure 6. Fourier transform magnitude of k^2-weighted Co K-edge EXAFS spectra of Co^{2+}@NH$_3$-C-C$_3$N$_4$ at high (43.3 μmol/mg) and low (2.3 μmol/mg) cobalt loadings and Co^{2+}@NH$_3$-C$_3$N$_4$ (29.8 μmol/g) without C doping. The k-range used in Fourier transform was from 2 to 7 Å^{-1}.

S3) instead of those far from the doped C atoms (Co−N binding energy −358 kJ/mol, Table S3). This comparison suggests that Co SACs with shorter Co−N bond lengths should be more active in CO$_2$-reduction catalysis. Interestingly, the calculated Co−N bond length in Co^{2+}@C-C$_3$N$_4$ is very close to that in Co Cyclam (Figure 5b, c), which demonstrated similar activity in CO$_2$ reduction upon depositing on C-C$_3$N$_4$ (Figures 1 and S9).

These experimental results on the NH$_3$-treated samples support the prediction made using the simplified model shown in Figure 5. Therefore, appropriate C doping of C$_3$N$_4$ can enhance the photocatalytic properties of Co SACs by improving its photoresponse, inhibiting charge recombination, and altering the local coordination environment of the Co^{2+} sites. Based on this present study and the results by others, our future work is focused on the synthesis of a few-layer C-doped C$_3$N$_4$ that contains more uniform and well-defined coordination sites for highly active Co SACs. We will also carry out additional DFT studies to explore mechanisms of selective CO$_2$ reduction on the Co SACs.

4. CONCLUSIONS

In summary, we have carried out experimental and computational work to probe the structure of single Co^{2+} sites in C$_3$N$_4$ that demonstrated excellent activity and product selectivity toward photocatalytic CO$_2$ reduction. A model of Co−N$_{2+2}$ coordination at C$_3$N$_4$ edge sites was found to be the most probable structure. This structure was further supported by experimental results obtained using Co SACs in NH$_3$-treated C$_3$N$_4$ samples that contain more edge sites. We also explored how C doping enhances the photocatalytic activity of Co SACs in C$_3$N$_4$. A simplified model was proposed to explain the origin of the observed enhancement effect of C doping, which involves substituting some N atoms near the metal center with C atoms. Such substitution resulted in shorter (and stronger) Co−N bonds which could alter the catalytic activity of the Co SACs toward CO$_2$ reduction.

ASSOCIATED CONTENT

Ⓢ Supporting Information

The Supporting Information is available free of charge at https://pubs.acs.org/doi/10.1021/acs.jpcc.2c01216.

Supporting figures and tables, including structures employed in DFT calculations, fitting results of EXAFS spectra, and additional characterization data (PDF)

■ AUTHOR INFORMATION

Corresponding Authors

N. Aaron Deskins − *Department of Chemical Engineering, Worcester Polytechnic Institute, Worcester, Massachusetts 01609, United States;* ⓘ orcid.org/0000-0002-0041-7960; Email: nadeskins@wpi.edu

Anatoly I. Frenkel − *Department of Materials Science and Chemical Engineering, Stony Brook University, Stony Brook, New York 11794, United States; Division of Chemistry, Brookhaven National Laboratory, Upton, New York 11973, United States;* ⓘ orcid.org/0000-0002-5451-1207; Email: anatoly.frenkel@stonybrook.edu

Gonghu Li − *Department of Chemistry, University of New Hampshire, Durham, New Hampshire 03857, United States;* ⓘ orcid.org/0000-0002-2924-3597; Email: gonghu.li@unh.edu

Authors

Peipei Huang − *Department of Chemistry, University of New Hampshire, Durham, New Hampshire 03857, United States*

Jiahao Huang − *Department of Materials Science and Chemical Engineering, Stony Brook University, Stony Brook, New York 11794, United States*

Junying Li − *Department of Materials Science and Chemical Engineering, Stony Brook University, Stony Brook, New York 11794, United States*

Thang Duc Pham − *Department of Chemical Engineering, Worcester Polytechnic Institute, Worcester, Massachusetts 01609, United States*

Lei Zhang − *Department of Chemistry, University of Connecticut, Storrs, Connecticut 06269, United States*

Jie He − *Department of Chemistry, University of Connecticut, Storrs, Connecticut 06269, United States;* ⓘ orcid.org/0000-0003-0252-3094

Gary W. Brudvig − *Department of Chemistry, Yale University, New Haven, Connecticut 06520, United States;* ⓘ orcid.org/0000-0002-7040-1892

Complete contact information is available at:
https://pubs.acs.org/10.1021/acs.jpcc.2c01216

Notes

The authors declare no competing financial interest.

■ REFERENCES

(1) Gates, B. C.; Flytzani-Stephanopoulos, M.; Dixon, D. A.; Katz, A. Atomically dispersed supported metal catalysts: perspectives and suggestions for future research. *Catal. Sci. Technol.* **2017**, *7*, 4259−4275.

(2) Cui, X.; Li, W.; Ryabchuk, P.; Junge, K.; Beller, M. Bridging homogeneous and heterogeneous catalysis by heterogeneous single-metal-site catalysts. *Nat. Catal.* **2018**, *1*, 385−397.

(3) Wang, A.; Li, J.; Zhang, T. Heterogeneous single-atom catalysis. *Nat. Rev. Chem.* **2018**, *2*, 65−81.

(4) Ji, S.; Chen, Y.; Wang, X.; Zhang, Z.; Wang, D.; Li, Y. Chemical Synthesis of Single Atomic Site Catalysts. *Chem. Rev.* **2020**, *120*, 11900−11955.

(5) Kaiser, S. K.; Chen, Z.; Faust Akl, D.; Mitchell, S.; Pérez-Ramírez, J. Single-Atom Catalysts across the Periodic Table. *Chem. Rev.* **2020**, *120*, 11703−11809.

(6) Xi, J.; Jung, H. S.; Xu, Y.; Xiao, F.; Bae, J. W.; Wang, S. Synthesis Strategies, Catalytic Applications, and Performance Regulation of Single-Atom Catalysts. *Adv. Funct. Mater.* **2021**, *31*, No. 2008318.

(7) He, Y.; Liu, S.; Priest, C.; Shi, Q.; Wu, G. Atomically dispersed metal−nitrogen−carbon catalysts for fuel cells: advances in catalyst design, electrode performance, and durability improvement. *Chem. Soc. Rev.* **2020**, *49*, 3484−3524.

(8) Qin, R.; Liu, K.; Wu, Q.; Zheng, N. Surface Coordination Chemistry of Atomically Dispersed Metal Catalysts. *Chem. Rev.* **2020**, *120*, 11810−11899.

(9) Gao, C.; Low, J.; Long, R.; Kong, T.; Zhu, J.; Xiong, Y. Heterogeneous Single-Atom Photocatalysts: Fundamentals and Applications. *Chem. Rev.* **2020**, *120*, 12175−12216.

(10) Wang, Y.; Mao, J.; Meng, X.; Yu, L.; Deng, D.; Bao, X. Catalysis with Two-Dimensional Materials Confining Single Atoms: Concept, Design, and Applications. *Chem. Rev.* **2019**, *119*, 1806−1854.

(11) Wang, Q.; Liu, K.; Fu, J.; Cai, C.; Li, H.; Long, Y.; Chen, S.; Liu, B.; Li, H.; Li, W.; et al. Atomically Dispersed s-Block Magnesium Sites for Electroreduction of CO_2 to CO. *Angew. Chem., Int. Ed.* **2021**, *60*, 25241−25245.

(12) Fu, J.; Liu, K.; Jiang, K.; Li, H.; An, P.; Li, W.; Zhang, N.; Li, H.; Xu, X.; Zhou, H.; et al. Graphitic Carbon Nitride with Dopant Induced Charge Localization for Enhanced Photoreduction of CO_2 to CH_4. *Adv. Sci.* **2019**, *6*, No. 1900796.

(13) Li, X.; Bi, W.; Chen, M.; Sun, Y.; Ju, H.; Yan, W.; Zhu, J.; Wu, X.; Chu, W.; Wu, C.; Xie, Y. Exclusive Ni-N4 Sites Realize Near-Unity CO Selectivity for Electrochemical CO_2 Reduction. *J. Am. Chem. Soc.* **2017**, *139*, 14889−14892.

(14) Li, Y.; Wang, S.; Wang, X.-s.; He, Y.; Wang, Q.; Li, Y.; Li, M.; Yang, G.; Yi, J.; Lin, H.; et al. Facile Top-Down Strategy for Direct Metal Atomization and Coordination Achieving a High Turnover Number in CO_2 Photoreduction. *J. Am. Chem. Soc.* **2020**, *142*, 19259−19267.

(15) Wang, X.; Chen, X.; Thomas, A.; Fu, X.; Antonietti, M. Metal-Containing Carbon Nitride Compounds: A New Functional Organic-Metal Hybrid Material. *Adv. Mater.* **2009**, *21*, 1609−1612.

(16) Cao, S.; Low, J.; Yu, J.; Jaroniec, M. Polymeric Photocatalysts Based on Graphitic Carbon Nitride. *Adv. Mater.* **2015**, *27*, 2150−2176.

(17) Xia, T.; Long, R.; Gao, C.; Xiong, Y. Design of atomically dispersed catalytic sites for photocatalytic CO_2 reduction. *Nanoscale* **2019**, *11*, 11064−11070.

(18) Li, Y.; Kong, T.; Shen, S. Artificial Photosynthesis with Polymeric Carbon Nitride: When Meeting Metal Nanoparticles, Single Atoms, and Molecular Complexes. *Small* **2019**, *15*, No. 1900772.

(19) Zhao, M.; Feng, J.; Yang, W.; Song, S.; Zhang, H. Recent Advances in Graphitic Carbon Nitride Supported Single-Atom Catalysts for Energy Conversion. *ChemCatChem* **2021**, *13*, 1250−1270.

(20) Xiao, X.; Zhang, L.; Meng, H.; Jiang, B.; Fu, H. Single Metal Atom Decorated Carbon Nitride for Efficient Photocatalysis: Synthesis, Structure, and Applications. *Solar RRL* **2021**, *5*, No. 2000609.

(21) Fang, Y.; Wang, X. Photocatalytic CO_2 conversion by polymeric carbon nitrides. *Chem. Commun.* **2018**, *54*, 5674−5687.

(22) Kuriki, R.; Matsunaga, H.; Nakashima, T.; Wada, K.; Yamakata, A.; Ishitani, O.; Maeda, K. Nature-Inspired, Highly Durable CO_2 Reduction System Consisting of a Binuclear Ruthenium(II) Complex and an Organic Semiconductor Using Visible Light. *J. Am. Chem. Soc.* **2016**, *138*, 5159−5170.

(23) Cometto, C.; Kuriki, R.; Chen, L.; Maeda, K.; Lau, T.-C.; Ishitani, O.; Robert, M. A Carbon Nitride/Fe Quaterpyridine Catalytic System for Photostimulated CO_2-to-CO Conversion with Visible Light. *J. Am. Chem. Soc.* **2018**, *140*, 7437−7440.

(24) Roy, S.; Reisner, E. Visible-Light-Driven CO_2 Reduction by Mesoporous Carbon Nitride Modified with Polymeric Cobalt Phthalocyanine. *Angew. Chem., Int. Ed.* **2019**, *58*, 12180−12184.

(25) Huang, P.; Pantovich, S. A.; Okolie, N. O.; Deskins, N. A.; Li, G. Hybrid Carbon Dioxide Reduction Photocatalysts Consisting of Macrocyclic Cobalt(III) Complexes Deposited on Semiconductor Surfaces. *ChemPhotoChem* **2020**, *4*, 420−426.

(26) Ma, B.; Chen, G.; Fave, C.; Chen, L.; Kuriki, R.; Maeda, K.; Ishitani, O.; Lau, T.-C.; Bonin, J.; Robert, M. Efficient Visible-Light-Driven CO_2 Reduction by a Cobalt Molecular Catalyst Covalently Linked to Mesoporous Carbon Nitride. *J. Am. Chem. Soc.* **2020**, *142*, 6188−6195.

(27) Huang, P.; Huang, J.; Pantovich, S. A.; Carl, A. D.; Fenton, T. G.; Caputo, C. A.; Grimm, R. L.; Frenkel, A. I.; Li, G. Selective CO_2 Reduction Catalyzed by Single Cobalt Sites on Carbon Nitride under Visible-Light Irradiation. *J. Am. Chem. Soc.* **2018**, *140*, 16042−16047.

(28) Wang, J.; Heil, T.; Zhu, B.; Tung, C.-W.; Yu, J.; Chen, H. M.; Antonietti, M.; Cao, S. A Single Cu-Center Containing Enzyme-Mimic Enabling Full Photosynthesis under CO_2 Reduction. *ACS Nano* **2020**, *14*, 8584−8593.

(29) Yang, Y.; Li, F.; Chen, J.; Fan, J.; Xiang, Q. Single Au Atoms Anchored on Amino-Group-Enriched Graphitic Carbon Nitride for Photocatalytic CO_2 Reduction. *ChemSusChem* **2020**, *13*, 1979−1985.

(30) Cheng, L.; Yin, H.; Cai, C.; Fan, J.; Xiang, Q. Single Ni Atoms Anchored on Porous Few-Layer g-C_3N_4 for Photocatalytic CO_2 Reduction: The Role of Edge Confinement. *Small* **2020**, *16*, No. 2002411.

(31) Li, Y.; Li, B.; Zhang, D.; Cheng, L.; Xiang, Q. Crystalline Carbon Nitride Supported Copper Single Atoms for Photocatalytic CO_2 Reduction with Nearly 100% CO Selectivity. *ACS Nano* **2020**, *14*, 10552−10561.

(32) Chen, P.; Lei, B.; Dong, Xa.; Wang, H.; Sheng, J.; Cui, W.; Li, J.; Sun, Y.; Wang, Z.; Dong, F. Rare-Earth Single-Atom La−N Charge-Transfer Bridge on Carbon Nitride for Highly Efficient and Selective Photocatalytic CO_2 Reduction. *ACS Nano* **2020**, *14*, 15841−15852.

(33) Ji, S.; Qu, Y.; Wang, T.; Chen, Y.; Wang, G.; Li, X.; Dong, J.; Chen, Q.; Zhang, W.; Zhang, Z.; et al. Rare-Earth Single Erbium Atoms for Enhanced Photocatalytic CO_2 Reduction. *Angew. Chem., Int. Ed.* **2020**, *59*, 10651−10657.

(34) Fu, J.; Zhu, L.; Jiang, K.; Liu, K.; Wang, Z.; Qiu, X.; Li, H.; Hu, J.; Pan, H.; Lu, Y.-R.; et al. Activation of CO_2 on graphitic carbon nitride supported single-atom cobalt sites. *Chem. Eng. J.* **2021**, *415*, No. 128982.

(35) Zhao, Z.; Liu, W.; Shi, Y.; Zhang, H.; Song, X.; Shang, W.; Hao, C. An insight into the reaction mechanism of CO_2 photoreduction catalyzed by atomically dispersed Fe atoms supported on graphitic carbon nitride. *Phys. Chem. Chem. Phys.* **2021**, *23*, 4690−4699.

(36) Zhang, J.-H.; Yang, W.; Zhang, M.; Wang, H.-J.; Si, R.; Zhong, D.-C.; Lu, T.-B. Metal-organic layers as a platform for developing single-atom catalysts for photochemical CO_2 reduction. *Nano Energy* **2021**, *80*, No. 105542.

(37) Xiao, X.; Gao, Y.; Zhang, L.; Zhang, J.; Zhang, Q.; Li, Q.; Bao, H.; Zhou, J.; Miao, S.; Chen, N.; et al. A Promoted Charge Separation/Transfer System from Cu Single Atoms and C_3N_4 Layers for Efficient Photocatalysis. *Adv. Mater.* **2020**, *32*, No. 2003082.

(38) Cao, Y.; Chen, S.; Luo, Q.; Yan, H.; Lin, Y.; Liu, W.; Cao, L.; Lu, J.; Yang, J.; Yao, T.; Wei, S. Atomic-Level Insight into Optimizing the Hydrogen Evolution Pathway over a Co1-N4 Single-Site Photocatalyst. *Angew. Chem., Int. Ed.* **2017**, *56*, 12191−12196.

(39) Chen, Z.; Mitchell, S.; Vorobyeva, E.; Leary, R. K.; Hauert, R.; Furnival, T.; Ramasse, Q. M.; Thomas, J. M.; Midgley, P. A.; Dontsova, D.; et al. Stabilization of Single Metal Atoms on Graphitic Carbon Nitride. *Adv. Funct. Mater.* **2017**, *27*, No. 1605785.

(40) Yu, F.; Huo, T.; Deng, Q.; Wang, G.; Xia, Y.; Li, H.; Hou, W. Single-atom cobalt-hydroxyl modification of polymeric carbon nitride for highly enhanced photocatalytic water oxidation: ball milling increased single atom loading. *Chem. Sci.* **2022**, *13*, 754−762.

(41) Li, J.; Zhao, S.; Yang, S.-Z.; Wang, S.; Sun, H.; Jiang, S. P.; Johannessen, B.; Liu, S. Atomically dispersed cobalt on graphitic carbon nitride as a robust catalyst for selective oxidation of ethylbenzene by peroxymonosulfate. *J. Mater. Chem. A* **2021**, *9*, 3029−3035.

(42) Chu, C.; Zhu, Q.; Pan, Z.; Gupta, S.; Huang, D.; Du, Y.; Weon, S.; Wu, Y.; Muhich, C.; Stavitski, E.; et al. Spatially separating redox centers on 2D carbon nitride with cobalt single atom for photocatalytic H_2O_2 production. *Proc. Natl. Acad. Sci.* **2020**, *117*, 6376−6382.

(43) Liu, W.; Hu, W.; Yang, L.; Liu, J. Single cobalt atom anchored on carbon nitride with well-defined active sites for photo-enzyme catalysis. *Nano Energy* **2020**, *73*, No. 104750.

(44) Xiong, Y.; Sun, W.; Han, Y.; Xin, P.; Zheng, X.; Yan, W.; Dong, J.; Zhang, J.; Wang, D.; Li, Y. Cobalt single atom site catalysts with ultrahigh metal loading for enhanced aerobic oxidation of ethylbenzene. *Nano Res.* **2021**, *14*, 2418−2423.

(45) Pollak, N.; Huang, P.; Bell, H.; Li, G.; Caputo, C. A. Tunable Photocatalytic Production of Syngas Using Co@C_3N_4 and Black Phosphorus. *ChemPhotoChem* **2021**, *5*, 674−679.

(46) Huang, P.; Huang, J.; Li, J.; Zhang, L.; He, J.; Caputo, C. A.; Frenkel, A. I.; Li, G. Effect of Carbon Doping on CO_2-Reduction Activity of Single Cobalt Sites in Graphitic Carbon Nitride. *ChemNanoMat* **2021**, *7*, 1051−1056.

(47) Jin, T.; Liu, C.; Li, G. Photocatalytic CO_2 reduction using a molecular cobalt complex deposited on TiO_2 nanoparticles. *Chem. Commun.* **2014**, *50*, 6221−6224.

(48) Kresse, G.; Hafner, J. Ab-Initio Molecular-Dynamics Simulation of the Liquid-Metal Amorphous-Semiconductor Transition in Germanium. *Phys. Rev. B* **1994**, *49*, 14251−14269.

(49) Kresse, G.; Hafner, J. Abinitio Molecular-Dynamics for Liquid-Metals. *Phys. Rev. B* **1993**, *47*, 558−561.

(50) Kresse, G.; Furthmuller, J. Efficient iterative schemes for ab initio total-energy calculations using a plane-wave basis set. *Phys. Rev. B* **1996**, *54*, 11169−11186.

(51) Kresse, G.; Furthmuller, J. Efficiency of ab-initio total energy calculations for metals and semiconductors using a plane-wave basis set. *Comput. Mater. Sci.* **1996**, *6*, 15−50.

(52) Kresse, G.; Joubert, D. From ultrasoft pseudopotentials to the projector augmented-wave method. *Phys. Rev. B* **1999**, *59*, 1758−1775.

(53) Blöchl, P. E. Projector augmented-wave method. *Phys. Rev. B* **1994**, *50*, 17953−17979.

(54) Perdew, J. P.; Burke, K.; Ernzerhof, M. Generalized gradient approximation made simple. *Phys. Rev. Lett.* **1996**, *77*, 3865−3868.

(55) Grimme, S.; Ehrlich, S.; Goerigk, L. Effect of the damping function in dispersion corrected density functional theory. *J. Comput. Chem.* **2011**, *32*, 1456−1465.

(56) Grimme, S.; Antony, J.; Ehrlich, S.; Krieg, H. A consistent and accurate ab initio parametrization of density functional dispersion correction (DFT-D) for the 94 elements H-Pu. *J. Chem. Phys.* **2010**, *132*, 154104.

(57) Kroke, E.; Schwarz, M.; Horath-Bordon, E.; Kroll, P.; Noll, B.; Norman, A. D. Tri-s-triazine derivatives. Part I. From trichloro-tri-s-triazine to graphitic C_3N_4 structures. *New J. Chem.* **2002**, *26*, 508−512.

(58) Ma, X.; Lv, Y.; Xu, J.; Liu, Y.; Zhang, R.; Zhu, Y. A Strategy of Enhancing the Photoactivity of g-C_3N_4 via Doping of Nonmetal Elements: A First-Principles Study. *J. Phys. Chem. C* **2012**, *116*, 23485−23493.

(59) Wu, H.-Z.; Zhong, Q.-H.; Bandaru, S.; Liu, J.; Lau, W. M.; Li, L.-L.; Wang, Z. Exploring the formation and electronic structure properties of the g-C_3N_4 nanoribbon with density functional theory. *J. Phys.: Condens. Matter* **2018**, *30*, No. 155303.

(60) Pan, F.; Zhang, H.; Liu, K.; Cullen, D.; More, K.; Wang, M.; Feng, Z.; Wang, G.; Wu, G.; Li, Y. Unveiling Active Sites of CO_2 Reduction on Nitrogen-Coordinated and Atomically Dispersed Iron and Cobalt Catalysts. *ACS Catal.* **2018**, *8*, 3116−3122.

(61) Li, J.; Zhang, H.; Samarakoon, W.; Shan, W.; Cullen, D. A.; Karakalos, S.; Chen, M.; Gu, D.; More, K. L.; Wang, G.; et al. Thermally Driven Structure and Performance Evolution of Atomically Dispersed FeN4 Sites for Oxygen Reduction. *Angew. Chem., Int. Ed.* **2019**, *58*, 18971−18980.

(62) Qin, X.; Zhu, S.; Xiao, F.; Zhang, L.; Shao, M. Active Sites on Heterogeneous Single-Iron-Atom Electrocatalysts in CO_2 Reduction Reaction. *ACS Energy Lett.* **2019**, *4*, 1778−1783.

(63) Li, Y.; Wu, S.; Huang, L.; Wang, J.; Xu, H.; Li, H. Synthesis of carbon-doped g-C_3N_4 composites with enhanced visible-light photo-catalytic activity. *Mater. Lett.* **2014**, *137*, 281−284.

(64) Aquino de Carvalho, N.; Wang, Y.; Morales-Soto, N.; Waldeck, D.; Bibby, K.; Doudrick, K.; Gilbertson, L. M. Using C-Doping to Identify Photocatalytic Properties of Graphitic Carbon Nitride That Govern Antibacterial Efficacy. *ACS ES&T Water* **2021**, *1*, 269−280.

(65) Chuang, P.-K.; Wu, K.-H.; Yeh, T.-F.; Teng, H. Extending the π-Conjugation of g-C_3N_4 by Incorporating Aromatic Carbon for Photocatalytic H2 Evolution from Aqueous Solution. *ACS Sustainable Chem. Eng.* **2016**, *4*, 5989−5997.

(66) Wang, Y.; Bai, X.; Qin, H.; Wang, F.; Li, Y.; Li, X.; Kang, S.; Zuo, Y.; Cui, L. Facile One-Step Synthesis of Hybrid Graphitic Carbon Nitride and Carbon Composites as High-Performance Catalysts for CO_2 Photocatalytic Conversion. *ACS Appl. Mater. Interfaces* **2016**, *8*, 17212−17219.

(67) Che, W.; Cheng, W.; Yao, T.; Tang, F.; Liu, W.; Su, H.; Huang, Y.; Liu, Q.; Liu, J.; Hu, F.; et al. Fast Photoelectron Transfer in $(C_{ring})−C_3N_4$ Plane Heterostructural Nanosheets for Overall Water Splitting. *J. Am. Chem. Soc.* **2017**, *139*, 3021−3026.

(68) Jiang, L.; Yuan, X.; Pan, Y.; Liang, J.; Zeng, G.; Wu, Z.; Wang, H. Doping of graphitic carbon nitride for photocatalysis: A reveiw. *Appl. Catal., B* **2017**, *217*, 388−406.

(69) Chen, Z.; Fan, T.-T.; Yu, X.; Wu, Q.-L.; Zhu, Q.-H.; Zhang, L.-Z.; Li, J.-H.; Fang, W.-P.; Yi, X.-D. Gradual carbon doping of graphitic carbon nitride towards metal-free visible light photocatalytic hydrogen evolution. *J. Mater. Chem. A* **2018**, *6*, 15310−15319.

(70) Liu, G.; Xue, M.; Liu, Q.; Yang, H.; Zhou, Y. Carbon doped honeycomb-like graphitic carbon nitride for photocatalytic hydrogen production. *J. Colloid Interface Sci.* **2019**, *552*, 728−734.

(71) Matsuoka, S.; Yamamoto, K.; Ogata, T.; Kusaba, M.; Nakashima, N.; Fujita, E.; Yanagida, S. Efficient and selective electron mediation of cobalt complexes with cyclam and related macrocycles in the p-terphenyl-catalyzed photoreduction of carbon dioxide. *J. Am. Chem. Soc.* **1993**, *115*, 601−609.

(72) Ogata, T.; Yanagida, S.; Brunschwig, B. S.; Fujita, E. Mechanistic and Kinetic Studies of Cobalt Macrocycles in a Photochemical CO_2 Reduction System: Evidence of Co-CO2 Adducts as Intermediates. *J. Am. Chem. Soc.* **1995**, *117*, 6708−6716.

■ **NOTE ADDED AFTER ASAP PUBLICATION**

This paper was published ASAP on May 13, 2022. Additional changes were made to Table 1, and corrected version was reposted on May 16, 2022.

📖 **Recommended by ACS**

Adsorption and Diffusion of CO on Clean and CO2-Precovered ZnO(10$\bar{1}$0)

Hong Shi, Xiang Shao, *et al.*

APRIL 04, 2018
THE JOURNAL OF PHYSICAL CHEMISTRY C   READ ☑

Adsorption of D2O and CO on Co3O4(111): Water Stabilizes Coadsorbed CO

Georg Fickenscher, Jörg Libuda, *et al.*

NOVEMBER 29, 2021
THE JOURNAL OF PHYSICAL CHEMISTRY C   READ ☑

Surface Structure of Co3O4 (111) under Reactive Gas-Phase Environments

George Yan and Philippe Sautet

JUNE 04, 2019
ACS CATALYSIS   READ ☑

CO Adsorbate Promotes Polaron Photoactivity on the Reduced Rutile TiO2(110) Surface

Cheng Cheng, Oleg V. Prezhdo, *et al.*

DECEMBER 30, 2021
JACS AU   READ ☑

Get More Suggestions >